American Mineralogist, Volume 110, pages 506–512, 2025

Magnetic collapse and low conductivity of Fe_3N in the deep interiors of Earth-like planets

Yukai Zhuang[1,2,‡], Jin Liu[3,4,*,†], Chaojia Lv[3,5,§], Liangxu Xu[5], Wenli Bi[6], Qingyang Hu[5,‖], Dongzhou Zhang[7,#], Gaston Garbarino[8], Shengcai Zhu[9,*], and Youjun Zhang[1,2,**]

[1]Institute of Atomic and Molecular Physics, Sichuan University, Chengdu 610065, China
[2]State Key Laboratory of Intelligent Construction and Healthy Operation and Maintenance of Deep Underground Engineering, Sichuan University, Chengdu, 610065, China
[3]Center for High Pressure Science, State Key Laboratory of Metastable Materials Science and Technology, Yanshan University, Qinhuangdao 066004, China
[4]CAS Center for Excellence in Deep Earth Science, Guangzhou 510640, China
[5]Center for High Pressure Science and Technology Advanced Research, Beijing 100193, China
[6]Department of Physics, University of Alabama at Birmingham, Birmingham, Alabama 35233, U.S.A.
[7]Hawai'i Institute of Geophysics and Planetology, School of Ocean and Earth Science and Technology, University of Hawai'i at Manoa, Honolulu, Hawaii 96822, U.S.A.
[8]ESRF-European Synchrotron Radiation Facility, 71 Avenue des Martyrs, CS40220, 38043 Grenoble Cedex, France
[9]School of Materials, Sun Yat-sen University, Guangzhou 510275, China

Abstract

The high-pressure behavior of iron nitrides has garnered significant attention due to the potential of deep nitrogen reservoirs within the Earth's interior. Here, we investigate the magnetic, structural, electrical, and thermal properties of Fe_3N up to 62 GPa and 2100 K, using multiple probes (including synchrotron X-ray diffraction, synchrotron Mössbauer spectroscopy, and electrical measurements) coupled with the diamond-anvil cell technique. Fe_3N undergoes a magnetic phase transformation from the ferromagnetic to paramagnetic state at ~17–20 GPa, 300 K. The equation of state was determined as $V_0/Z = 42.8(1)$ Å^3, and $K_0 = 151.8(1)$ GPa, with K' fixed at 4. Additionally, Fe_3N exhibits unexpectedly low electrical and thermal conductivity under high-pressure and high-temperature conditions. This result suggests that deep nitrogen cycling may contribute to the thermal evolution of the deep interiors of Earth and other terrestrial bodies.

Keywords: Deep nitrogen cycling, Fe_3N, synchrotron X-ray diffraction, synchrotron Mössbauer spectroscopy, transport properties, Physics and Chemistry of Earth's Deep Mantle and Core

Introduction

Nitrogen is a highly abundant element in the Solar System and has garnered increasing attention in the field of geoscience (Bebout et al. 2013). Molecular N_2 is the primary constituent of the current atmosphere, but the presence and movement of nitrogen within the Earth's deep interior is a topic of intense debate (Halliday 2013). Some stony meteorites have suggested that negligible amounts of nitrogen exist within the Earth's interior, with only several parts per million (ppm) detected (Sugiura et al. 1998; Allègre et al. 2001). However, carbonaceous and enstatite chondrites, which are the primary building blocks of the Earth, can contain more than 1 wt% nitrogen (Javoy 1997; Moore et al. 1969). Additionally, iron meteorites and mantle-derived diamonds in kimberlites and metamorphic rocks have been found to contain more than 1 wt% nitrogen (Sugiura et al. 1998; Cartigny 2005). Nitrogen serves as a sensitive tracer of volatile exchanges between planetary interiors and outer space (Mao and Mao 2020). Over time, the nitrogen content of the Earth's surface may have varied significantly due to interactions with the deep Earth or by escaping into outer space (Marty et al. 2013; Shi et al. 2022). Although the amount of escaping nitrogen is still unclear, a significant amount of nitrogen is likely trapped inside the Earth's interior, approximately twice the current atmospheric nitrogen level (Pepin 2006; Goldblatt et al. 2009).

Ammonium-bearing sediments and altered oceanic crusts are the primary sources of nitrogen that enter the Earth's interior. In subduction zones with low temperatures, subducted nitrogen can reach the depths beneath island arcs (Busigny et al. 2003; Watenphul et al. 2010; Sokol et al. 2017a). Molecular nitrogen is highly incompatible and is likely to be outgassed from the deep Earth. Conversely, ammonium may play a dominant role in some aqueous fluids in the Earth's interior (Zerkle and Mikhail 2017). Experiments and thermodynamic calculations show that metallic iron Fe^0 may reach ~0.1–0.5 wt% at depths >250 km (Frost et al. 2004; Rohrbach et al. 2007). Furthermore, nitrogen is a siderophile element under reducing conditions, and it is more likely to form iron nitrides through reactions between metallic iron and nitrogen-bearing compounds in the deep Earth. Due to the high solubility of nitrogen in iron at high pressure, the amount of deep nitrogen in the Earth's mantle and core could be significantly underestimated (Litasov et al. 2017).

The Fe-N binary system exhibits a complex and diverse phase diagram, with various stoichiometries of iron nitrides such

* Co-corresponding author E-mails: jinliu@ysu.edu.cn, zhushc@mail.sysu.edu.cn
† Special collection papers can be found online at our website in the Special Collection section.
‡ Orcid https://orcid.org/0000-0002-5448-6881
§ Orcid https://orcid.org/0000-0001-8831-8555
‖ Orcid https://orcid.org/0000-0002-2742-3017
Orcid https://orcid.org/0000-0002-6679-892X
** Orcid https://orcid.org/0000-0001-5340-4170

as cubic FeN and γ-Fe_4N, tetragonal α-$Fe_{16}N_2$, hexagonal/orthorhombic Fe_2N, hexagonal Fe_7N_3, and ε-Fe_3N (Yin et al. 2014; Minobe et al. 2015). The transformation of γ-Fe_4N to ε-$Fe_3N_{0.75}$ occurs at 8.5 GPa and 1373 K (Guo et al. 2013). ζ-Fe_2N undergoes a structural transition to form ε-$Fe_3N_{1.5}$ at 15 GPa and 1600 K (Schwarz et al. 2009). Fe_7N_3 may be stable under high-pressure-temperature (*P-T*) conditions relevant to the core-mantle boundary (Kusakabe et al. 2019; Sagatov et al. 2019), and Fe_3N can be stable at 1473 K and 30 GPa (Litasov et al. 2017). It is noteworthy that ε-Fe_3N can accommodate up to 2.5 wt% carbon at 1600 K and 7.8 GPa (Sokol et al. 2017b), indicating the possibility of substitutional solid solutions of iron nitride and carbide in the Earth's interior (Johnson and Goldblatt 2015; Sagatov et al. 2019). ε-Fe_3N is a crucial nitrogen-bearing phase, and understanding its phase relation, compressibility, and conductivity properties at high pressure is essential to deciphering the coevolution of nitrogen and carbon cycles in the deep Earth. However, the high-*P-T* behavior of Fe_3N, including its magnetic, thermal, and electrical conductivity, has not been extensively studied.

In this study, we systematically investigated the magnetic transition, equation of state (EoS), and electrical conductivity (EC) of Fe_3N up to 62 GPa and 2100 K using diamond-anvil cell (DAC) techniques in combination with synchrotron X-ray diffraction (XRD), synchrotron Mössbauer spectroscopy (SMS), and the four-probe method of electrical measurements (van der Pauw 1958). Our results indicate a ferromagnetic-paramagnetic phase transition of Fe_3N at 17–20 GPa. Additionally, similar to other iron-light element alloys, such as Fe_3C and Fe_3Si, the incorporation of N significantly reduces the density and conductivity of Fe. These findings highlight the crucial role of Fe_3N in the deep interiors of Earth and other terrestrial planets.

Experimental Methods

The polycrystalline ε-Fe_3N sample (Lot#: RA191101) was procured from Antechnology Co., Ltd, Beijing. In situ angular-dispersive XRD experiments were conducted on Fe_3N at room temperature at the 13BM-C beamline of the GeoSoilEnviroCARS (GSECARS) at the Advanced Phonon Source (APS). A tungsten foil was utilized as the gasket, which was pre-indented to a thickness of ~50 μm. A sample chamber was created by drilling a 100 μm center hole. The sample powder was ground and pre-compressed into a platelet of dimensions ~10 (T) × 50 (W) × 50 (L) μm^3 and then placed into the 200 μm culet DAC chamber. Neon gas was selected as the pressure medium and introduced into the chamber. To ensure the pressure, a ruby sphere and Au were placed near the Fe_3N sample. The pressure was obtained via the shift of ruby R_1 emission line with pressure and the EoS of Au (Mao et al. 1986; Ye et al. 2018). The pressure uncertainty was <1 GPa.

XRD measurements at 300 K were performed using a highly monochromatized X-ray beam with a wavelength of 0.434 Å. The X-ray beam was focused to a beam size of ~15 μm (full-width at half maximum, FWHM) at the sample chamber. The calibration of the sample-to-detector distance, rotation angle with respect to the X-ray beam, and tilt angle were carried out using LaB_6 powder. Diffraction patterns were recorded using a MAR CCD detector with an exposure time of 120 s. XRD images were obtained at intervals of 1–3 GPa. The XRD pattern at 33.1 GPa and 2000 K was obtained at the beamline ID15B of the European Synchrotron Radiation Facility (ESRF). The energy of the monochromatized X-ray beam is 88.54 KeV with a wavelength of 0.140 Å and beam size of ~10 μm in diameter. Diffraction data sets were collected on a large area EIGER2 X 9M CdTe flat panel detector with the omega scan range from −10° to +10°. Pressure was determined by calibrating the ruby fluorescence line shift in an offline ruby system. The lattice parameters and volumes of the sample were determined from the diffraction lines using the Dioptas and Unit Cell programs (Prescher and Prakapenka 2015). The pressure-volume (*P-V*) profile of the sample was fitted using the third-order Birch-Murnaghan EoS with the EosFit7-Gui procedure (Gonzalez-Platas et al. 2016):

$$P = \frac{3}{2}K_0\left[\left(\frac{V_0}{V}\right)^{\frac{7}{3}} - \left(\frac{V_0}{V}\right)^{\frac{5}{3}}\right] \times \left\{1 + \frac{3}{4}(K' - 4)\left[\left(\frac{V_0}{V}\right)^{\frac{2}{3}} - 1\right]\right\} \quad (1)$$

where P represents the pressure, K_0 represents the isothermal bulk modulus at 1 bar, and K' represents the pressure derivative of K_0 at ambient pressure. V_0 denotes the unit-cell volume at ambient pressure, and V represents the volume at high pressure. When K' is fixed at a value of 4, the equation can be simplified to the second-order Birch-Murnaghan EoS.

High-pressure time-domain SMS experiments were conducted at beamline 16-IDD, APS, Argonne National Laboratory (ANL) at room temperature. A monochromatic X-ray beam with an energy of 14.41 keV, a band width of 2 meV, and a FWHM of 5–7 μm was employed to excite the ^{57}Fe nucleus in the Fe_3N sample (Sturhahn 2004; Liu et al. 2019). The time-delayed SMS spectra were recorded using an avalanche photodiode detector (APD) in the forward direction. Each SMS signal was collected for ~2 h. The pressure values were determined using the ruby fluorescence pressure scale before and after each measurement (Akahama and Kawamura 2010).

We conducted electrical resistance measurements using symmetric DACs with culets of 260 μm. To collect the resistance data, we employed a Keithley 2400 source meter and a Keithley 2182A nanovoltage meter. The output current ranged from 1 to 5 mA. Prior to the experiment, the tungsten gasket was pre-indented to a thickness of ~50 μm. Subsequently, we utilized a laser drilling system to create a 200 μm hole at the center of the pre-indentation. The boron nitride-epoxy mixture (in a ratio of 10:1) was then inserted into the 200 μm hole and pre-indented to a pressure of ~15 GPa, as determined by the ruby fluorescence pressure standard. Next, we employed the laser drilling system to create a hole with a diameter of 100 μm at the center of the boron nitride-epoxy inset gasket, which served as the insulating sample chamber. To establish electrical contact with the sample, we utilized four Pt foils with a thickness of <4 μm as electrodes. The four-terminal method, as described by van der Pauw (1958), was employed to minimize the influence of sample shape and contact resistance on electrical measurements under high pressure. For high-temperature experiments, the sample chamber had a diameter of ~30 μm, and the sample was sandwiched between two NaCl layers. High-temperature conditions were achieved using a double-sided laser heating system at the Center for High Pressure Science and Technology Advanced Research (HPSTAR). The system was equipped with two ytterbium CW fiber lasers operating at a wavelength of 1070 nm. The thickness of the sample was determined using a simple interpolation approach, as detailed in the methods section of Hou et al. (2021) and Zhuang et al. (2022).

Results and Discussion

Magnetic transition of Fe_3N at high pressure

The magnetic ordering of the iron 3*d* electrons in ε-Fe_3N was determined through SMS measurements conducted under high-pressure conditions. In this study, SMS signals of Fe_3N were obtained at room temperature up to 61.9 GPa (Fig. 1). The results indicate that Fe_3N maintains its ferromagnetic state, as evidenced by the presence of quantum beats resulting from nuclear Zeeman splitting, until a pressure of 16.6 GPa. Beyond this pressure, Fe_3N enters a paramagnetic state at approximately 20 GPa, characterized by the disappearance of multiple beats and the emergence of single-beat spectra. The paramagnetic state of Fe_3N persists at pressures up to 61.9 GPa at room temperature. The magnetic moment observed in ε-Fe_3N is attributed to an unbalanced charge distribution, with contributions from iron and nitrogen atoms. The density of states (DoS) of iron is primarily governed by its 3*d* states, which are mixed with the 2*p* DoS of nitrogen. This results in electron exchange processes with a covalent bonding nature between the Fe and N atoms (Panda and Gajbhiye 1997). Consequently, the nitrogen content at high pressure can influence the magnetization in the Fe-N system.

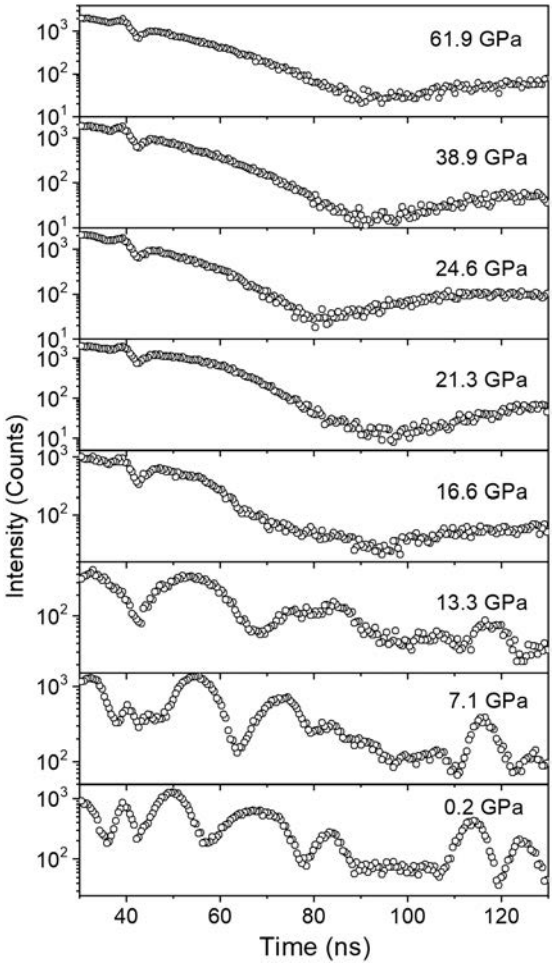

FIGURE 1. Representative SMS spectra at high pressure. Fe_3N loses magnetism around 16 GPa, as indicated by the disappearance of the multiple quantum beats. The symbols are larger than the experimental errors (±2SD).

The magnetism in Fe_3N is suppressed at approximately 20 GPa, which is consistent with the behavior of γ′-Fe_4N at 24 GPa, as reported by Ishimatsu et al. (2003). X-ray magnetic circular dichroism measurements confirmed the magnetic transition in γ′-Fe_4N, characterized by a loss of spin polarization. Additionally, Lv et al. (2020) found that Fe_7N_3 and Fe_4N transition from the ferromagnetic to paramagnetic state at pressures of 43 and 34 GPa, respectively. This pressure-induced ferromagnetic-to-paramagnetic transition appears to be a common phenomenon in iron nitrides such as $Fe_3N_{1.2}$ (Lv and Liu 2023). Similar magnetic transitions have also been observed in other iron alloys containing light elements such as carbon, phosphorus, and sulfur (Lin et al. 2004; Chen et al. 2014, 2018; Gu et al. 2016). In other words, the incorporation of light elements into iron affects the DoS of the material. These magnetic phase transitions occur in iron alloys at approximately 10–50 GPa.

Compressibility of Fe_3N at high pressure

XRD patterns were collected for the polycrystalline Fe_3N sample (Online Materials[1] Fig. S1) under various pressures up to 52.3 GPa (Fig. 2). The obtained XRD patterns were analyzed using the General Structure Analysis System (GSAS) to determine the atomic positions of Fe_3N (Online Materials[1] Table S1 and Fig. S2). The Fe_3N sample exhibited a trigonal structure (space group: $P312$) both at ambient conditions and under high pressures. Furthermore, the trigonal structure remained stable after heating up to 2000(200) K at 33.1 GPa, demonstrating that Fe_3N may exist along the geothermal temperature. The volume of Fe_3N was measured as a function of pressure at 300 K and is shown in Figure 3a. The P-V profile of Fe_3N displayed continuous compressibility with increasing pressure. Interestingly, the pressure-induced magnetic phase transition did not cause any visible discontinuity in the P-V profile within the 17–20 GPa range. Therefore, a single Birch-Murnaghan EoS was fitted to the entire P-V data from 0 to 52 GPa (Fig. 3a; Online Materials[1] Table S2). The fitting parameters were determined as follows: $V_0/Z = 42.8(1)$ Å^3 (where Z is the number of formula units in the unit cell, $Z = 2$), $K_0 = 151.78(10)$ GPa, and $K' = 4$. According to the unit-cell volume at ambient conditions, the V_0/Z value was 43.2(1) Å^3 for Fe_3N. The V_0 value of 86.4(2) Å^3 for Fe_3N is comparable to the value of 86.18 Å^3 obtained for $Fe_3N_{1.26}$ in previous multi-anvil experiments (Litasov et al. 2017). However, the K_0 value of Fe_3N is ~6.9% lower than that of $Fe_3N_{1.26}$ (163 GPa), while theoretical predictions suggested a K_0 value of 214 GPa for Fe_3N (Popov et al. 2015).

The compressibility of iron nitride at high pressure is generally similar to that of hexagonal close-packed (hcp) iron (Adler and Williams 2005; Fei et al. 2016; Litasov et al. 2017; Lv et al. 2020). However, Fe_3N is more compressible than pure hcp-Fe at high pressure, likely due to the softening of its lattice in the presence of light element (Fig. 3b). For example, the difference in volume changes ($\Delta V/V_0$) between pure iron and Fe_3N increases from ~0.022 at 17 GPa to 0.038 at 50 GPa. On the other hand, Fe_7C_3 undergoes elastic softening during the pressure-induced Invar transition before entering a stiffer paramagnetic state (Chen et al. 2012). Similarly, Fe_3C and Fe_3P become less compressible after the collapse of their magnetic moments (Prescher et al. 2012; Lai et al. 2020). Therefore, the compressibility of transition metal nitrides, carbides, and phosphides under high pressure is influenced by both their crystal structure and the presence of light elements.

High-pressure electrical and thermal conductivity of Fe_3N

The impact of high pressure on the electrical conductivity of Fe_3N was examined up to ~50 GPa (see Fig. 4 and Online Materials[1] Fig. S3). At 0.5 GPa and 300 K, the EC of Fe_3N was determined to be $9.75(95) \times 10^2$ S m^{-1} (Online Materials[1] Table S3). Similar to the volume-pressure relationship, the EC value continuously increases with rising pressure without any abrupt changes during 17–20 GPa. The EC of Fe_3N increases significantly at ~40 GPa, which may be induced by the spin transition of iron in Fe_3N. Additionally, the EC of Fe_3N was measured under simultaneous high-P-T conditions (Fig. 4b; Online Materials[1] Table S4). Due to its metallic nature, the EC of Fe_3N initially decreases with increasing temperature at high pressure but then exhibits an inverse trend at ~2000 K, likely due to melting.

The EC values of iron nitrides are significantly lower than those of iron-carbon, iron-nickel, iron-silicon, and iron-sulfur

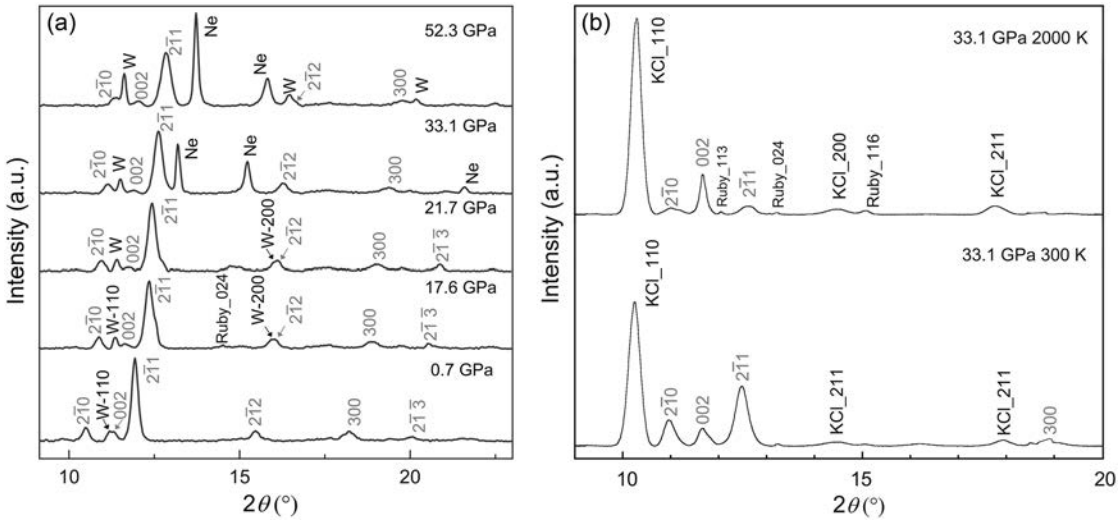

Figure 2. (**a**) Representative high-pressure X-ray diffraction patterns of ε-Fe_3N. Pure digital labels indicate the diffraction (*hkl*) lines of Fe_3N. The peaks of tungsten (W) are from the gasket. The pressure-transmitting medium is neon (Ne). The X-ray wavelength (λ): 0.4340 Å. (**b**) High-temperature pattern of ε-Fe_3N at 33.1 GPa. The pattern from 2000 K was obtained from quenched sample at ESRF. The pressure-transmitting medium is KCl. The X-ray wavelength (λ): 0.4102 Å.

alloys at room temperature, with a difference of ~2–3 orders of magnitude (Seagle et al. 2013; Gomi and Hirose 2015; Suehiro et al. 2017; Zhang et al. 2018; Zhuang et al. 2021). Fe_3N, in particular, exhibits even lower EC values than pure iron at geothermal temperatures. It can be attributed to the significant influence of nitrogen incorporation on the electronic structure of iron-rich alloys. The presence of nitrogen impurity in iron leads to a resonance effect, resulting in an increase in resistance (Fert and Campbell 1976).

Similar to Fe_3C (Zhang et al. 2018), the electronic thermal conductivity (TC) of metallic Fe_3N can be determined based on electron conduction using the Wiedemann-Franz law (Stacey and Loper 2007; de Koker et al. 2012). The equation for this relationship is as follows:

$$k_e = L\sigma T \quad (2)$$

where k_e represents the TC derived from electrons, L is the Lorenz number, σ represents the electrical conductivity, and T is the temperature. Under high-P-T conditions, the value of L is typically equal to 2.44×10^{-8} $W\Omega K^{-2}$, which is known as the ideal value of L_0 (Anderson 1998; Gomi and Hirose 2015; Ohta et al. 2016). The TC values for Fe_3C and Fe_7C_3 range from 5–10 Wm^{-1} K^{-1}, while pure iron has a TC of ~100 Wm^{-1} K^{-1} at 50 GPa and 300 K (Zhang et al. 2018). The presence of light elements in iron alloys significantly reduces the electronic TC of iron (Online Materials[1] Fig. S3a). Among these light elements, nitrogen has a significant alloying effect. The TC values of Fe_3N are lower than those of iron-carbon alloys and hcp-Fe within the investigated P-T range (Online Materials[1] Fig. S3). Nitrogen can efficiently reduce the

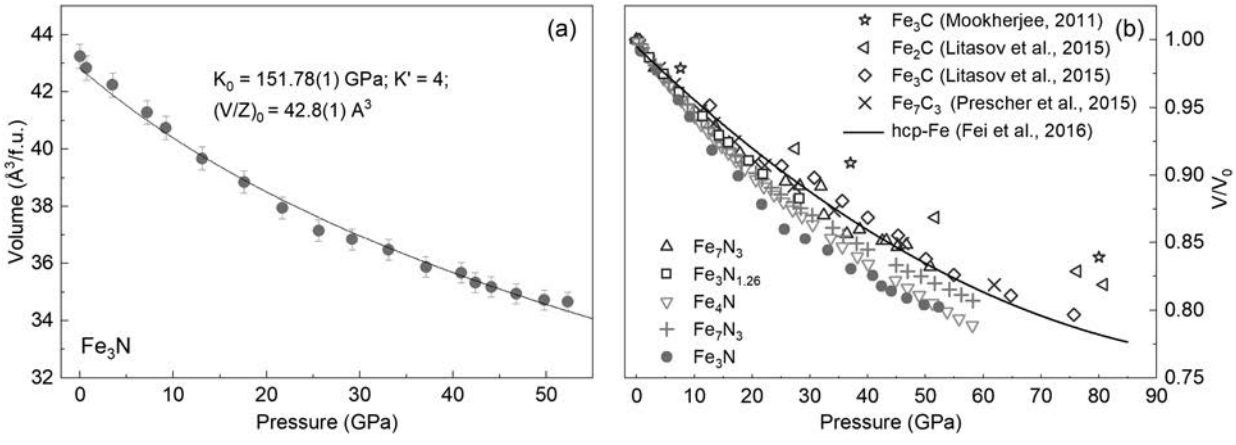

Figure 3. (**a**) The volume changes of Fe_3N phases with pressure. The solid curves represent the fitting to the P-V data based on the second-order Birch-Murnaghan. (**b**) Compression behavior of Fe_3N compared with other iron nitrides and iron carbides. Fe_7N_3 (triangle): Adler and Williams (2005); $Fe_3N_{1.26}$ (squares): Litasov et al. (2017); Fe_4N (inverted triangle) and Fe_7N_3 (cross): Lv et al. (2020); Fe_3N (solid circle): this study.

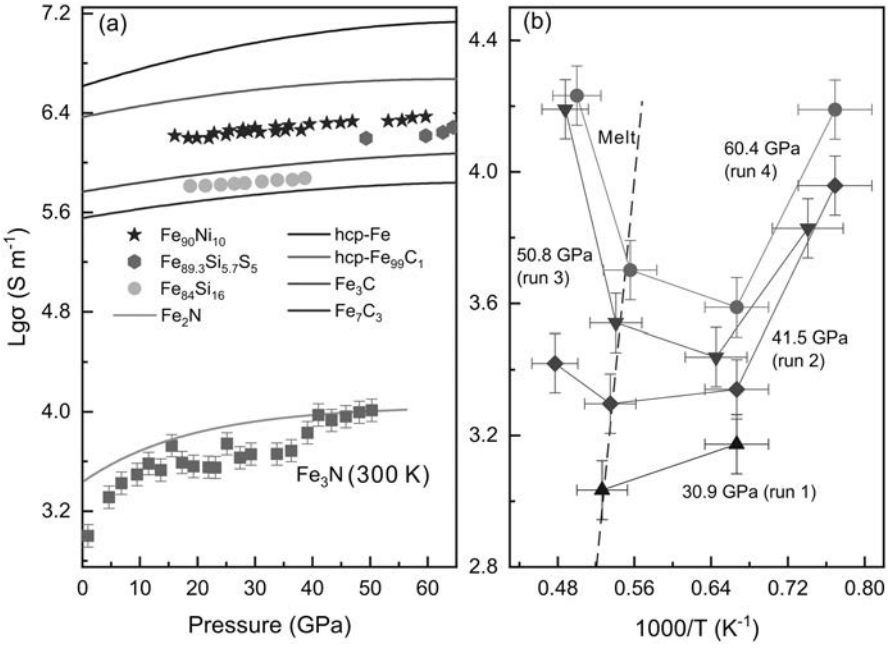

FIGURE 4. (**a**) The electrical conductivity (EC) of Fe_3N vs. pressure with other iron alloys at 300 K. Squares: Fe_3N (this study). Pentagons: $Fe_{90}Ni_{10}$ (Gomi and Hirose 2015). Hexagons and circles: $Fe_{89.3}Si_{5.7}S_5$ and $Fe_{84}Si_{16}$, respectively (Seagle et al. 2013). The dashed curve: Fe_2N (Zhuang et al. 2021). The solid, dotted dashed, double dotted dashed, and short dashed curves: hcp-Fe, hcp-$Fe_{99}C_1$, Fe_3C, and Fe_7C_3, respectively (Zhang et al. 2018). The error bars include uncertainties in the measured resistance and the relationship between the electrode contact length and the sample diameter (van der Pauw 1958), which is estimated to be <25%. (**b**) The EC of Fe_3N under high-pressure and -temperature conditions in this study. The high-temperature experiments were conducted for four runs at different high-pressure conditions. The temperature errors were mainly due to the high-temperature gradient under laser heating.

thermal properties of iron under high-*P-T* conditions. Incorporating nitrogen into iron can alter the stable crystalline structure and influence the magneto-elastic properties by controlling the electrons in 3*d* orbitals around Fe atoms (Widenmeyer et al. 2014; Sifkovits et al. 1999). These findings suggest that the presence of Fe_3N may significantly impact the thermal dynamics and evolution of the interiors of Earth.

IMPLICATIONS

Fe_3N exhibits a similar structure to Fe_3C and can form solid solutions with Fe_3C under high-*P-T* conditions (Sokol et al. 2017a; Litasov et al. 2017). The presence of abundant carbon in ε-Fe_3N does not alter its structure, resulting in the formation of iron carbonitride ε-$Fe_3(C,N)$ (Jack 1948). In Fe_3C, iron atoms adopt an hcp arrangement, while carbon atoms occupy a trigonal prismatic site. This configuration leads to a very low solubility of nitrogen in Fe_3C under ambient conditions. However, the solubility of nitrogen in Fe_3C increases with temperature. At 1625 K and 7.8 GPa, ε-Fe_3N can contain 1.9–2.7 wt% carbon, whereas the nitrogen concentration in Fe_3C is 0.5 wt% under the same *P-T* conditions (Sokol et al. 2017a; Lv and Liu 2022). Additionally, Fe, Fe_3C, and Fe_3N can approach chemical equilibrium at depths >250 km (Sokol et al. 2017a).

Furthermore, it has been observed that Fe_7N_3 exhibits a nearly identical structure and elasticity to Fe_7C_3 (Minobe et al. 2015; Li et al. 2016). The presence of carbon and nitrogen in metallic iron and iron carbonitrides in the deep Earth has been extensively documented (Dasgupta and Hirschmann 2010; Frost and McCammon 2008), indicating a coupling between the nitrogen and carbon cycles within the Earth's interior. Notably, although Fe-C and Fe-N alloys share the same crystal structures at high *P-T*, their conductivities should differ due to their dissimilar electronic structures. The nonmetallic property of N is stronger than that of C, given that the nuclear charge of N is larger and the attraction potential for the outermost electron is stronger with respect to C. Therefore, the conductivities of nitrogen alloys are lower than those of carbon alloys. The presence of Fe_3N can significantly reduce the electrical and thermal conductivity of iron. The XRD experiments conducted in our study have demonstrated the stability of Fe_3N under high-*P-T* conditions. This finding aligns with the previous observations that Fe_3N is a mineral inclusion in lower-mantle diamonds from Rio Soriso, Brazil (Kaminsky and Wirth 2017). Local enrichments of solid/molten Fe_3N may lead to thermal heterogeneity (e.g., local heating and inhomogeneous heat flow) in the deep Earth and other terrestrial planets. Additionally, the high-temperature stability of nickel nitrides, such as ε-Ni_3N, which share the same structure as iron nitrides, has been reported (Guillermet and Frisk 1991). The introduction of nickel may have influenced the co-evolution of nitrogen and carbon cycles in the deep Earth (Hirao et al. 2022), as the lattice of Fe_3C and Fe_7C_3 could become unstable with increasing nickel content (Rohrbach et al. 2014; Strong and Chrenko 1971).

ACKNOWLEDGMENTS AND FUNDING

We acknowledge Yuming Xiao and Paul Chow for assistance with the experiment at beamline 16-IDD, APS, ANL. This work is supported by NSFC Grant no. 42072052, 42150102, 42150101, and the Sichuan Science and Technology Program (Grant No. 2023NSFSC1910). 13BM-C is partially supported by COMPRES under NSF Cooperative Agreement EAR-1606856. GeoSoilEnviroCARS is supported by the NSF-Earth Sciences (EAR-1634415) and the DOE-GeoSciences (DE-FG02-94ER14466). HPCAT operations are supported by DOE-NNSA's Office of Experimental Sciences. This research used resources from the Advanced Photon Source, a U.S. Department of Energy (DOE) Office of Science User Facility operated for the DOE Office of Science by Argonne National Laboratory under Contract No. DE-AC02-06CH11357. Some experiments are supported by the Synergic Extreme Condition User Facility (SECUF).

References Cited

Adler, J.F. and Williams, Q. (2005) A high-pressure X-ray diffraction study of iron nitrides: Implications for Earth's core. Journal of Geophysical Research: Solid Earth, 110, B01203.

Akahama, Y. and Kawamura, H. (2010) Pressure calibration of diamond anvil Raman gauge to 410 GPa. Journal of Physics: Conference Series, 215, 012195, https://doi.org/10.1088/1742-6596/215/1/012195.

Allègre, C., Manhès, G., and Lewin, É. (2001) Chemical composition of the Earth and the volatility control on planetary genetics. Earth and Planetary Science Letters, 185, 49–69, https://doi.org/10.1016/S0012-821X(00)00359-9.

Anderson, O.L. (1998) The Grüneisen parameter for iron at outer core conditions and the resulting conductive heat and power in the core. Physics of the Earth and Planetary Interiors, 109, 179–197, https://doi.org/10.1016/S0031-9201(98)00123-X.

Bebout, G.E., Fogel, M.L., and Cartigny, P. (2013) Nitrogen: Highly volatile yet surprisingly compatible. Elements, 9, 333–338, https://doi.org/10.2113/gselements.9.5.333.

Busigny, V., Cartigny, P., Philippot, P., Ader, M., and Javoy, M. (2003) Massive recycling of nitrogen and other fluid-mobile elements (K, Rb, Cs, H) in a cold slab environment: Evidence from HP to UHP oceanic metasediments of the Schistes Lustrés nappe (western Alps, Europe). Earth and Planetary Science Letters, 215, 27–42, https://doi.org/10.1016/S0012-821X(03)00453-9.

Cartigny, P. (2005) Stable isotopes and the origin of diamond. Elements, 1, 79–84, https://doi.org/10.2113/gselements.1.2.79.

Chen, B., Gao, L., Lavina, B., Dera, P., Alp, E.E., Zhao, J., and Li, J. (2012) Magneto-elastic coupling in compressed Fe_7C_3 supports carbon in Earth's inner core. Geophysical Research Letters, 39, L18301, https://doi.org/10.1029/2012GL052875.

Chen, B., Li, Z., Zhang, D., Liu, J., Hu, M.Y., Zhao, J., Bi, W., Alp, E.E., Xiao, Y., Chow, P., and others. (2014) Hidden carbon in Earth's inner core revealed by shear softening in dense Fe_7C_3. Proceedings of the National Academy of Sciences of the United States of America, 111, 17755–17758, https://doi.org/10.1073/pnas.1411154111.

Chen, B., Lai, X., Li, J., Liu, J., Zhao, J., Bi, W., Ercan Alp, E., Hu, M.Y., and Xiao, Y. (2018) Experimental constraints on the sound velocities of cementite Fe_3C to core pressures. Earth and Planetary Science Letters, 494, 164–171, https://doi.org/10.1016/j.epsl.2018.05.002.

Dasgupta, R. and Hirschmann, M.M. (2010) The deep carbon cycle and melting in Earth's interior. Earth and Planetary Science Letters, 298, 1–13, https://doi.org/10.1016/j.epsl.2010.06.039.

de Koker, N., Steinle-Neumann, G., and Vlcek, V. (2012) Electrical resistivity and thermal conductivity of liquid Fe alloys at high P and T, and heat flux in Earth's core. Proceedings of the National Academy of Sciences of the United States of America, 109, 4070–4073, https://doi.org/10.1073/pnas.1111841109.

Fei, Y., Murphy, C., Shibazaki, Y., Shahar, A., and Huang, H. (2016) Thermal equation of state of hcp-iron: Constraint on the density deficit of Earth's solid inner core. Geophysical Research Letters, 43, 6837–6843, https://doi.org/10.1002/2016GL069456.

Fert, A. and Campbell, I.A. (1976) Electrical resistivity of ferromagnetic nickel and iron based alloys. Journal of Physics F: Metal Physics, 6, 849–871, https://doi.org/10.1088/0305-4608/6/5/025.

Frost, D.J. and McCammon, C.A. (2008) The redox state of Earth's mantle. Annual Review of Earth and Planetary Sciences, 36, 389–420, https://doi.org/10.1146/annurev.earth.36.031207.124322.

Frost, D.J., Liebske, C., Langenhorst, F., McCammon, C.A., Trønnes, R.G., and Rubie, D.C. (2004) Experimental evidence for the existence of iron-rich metal in the Earth's lower mantle. Nature, 428, 409–412, https://doi.org/10.1038/nature02413.

Goldblatt, C., Claire, M.W., Lenton, T.M., Matthews, A.J., Watson, A.J., and Zahnle, K.J. (2009) Nitrogen-enhanced greenhouse warming on early Earth. Nature Geoscience, 2, 891–896, https://doi.org/10.1038/ngeo692.

Gomi, H. and Hirose, K. (2015) Electrical resistivity and thermal conductivity of hcp Fe-Ni alloys under high pressure: Implications for thermal convection in the Earth's core. Physics of the Earth and Planetary Interiors, 247, 2–10, https://doi.org/10.1016/j.pepi.2015.04.003.

Gonzalez-Platas, J., Alvaro, M., Nestola, F., and Angel, R. (2016) EosFit7-GUI: A new graphical user interface for equation of state calculations, analyses and teaching. Journal of Applied Crystallography, 49, 1377–1382, https://doi.org/10.1107/S1600576716008050.

Gu, T., Fei, Y., Wu, X., and Qin, S. (2016) Phase stabilities and spin transitions of $Fe_3(S_{1-x}P_x)$ at high pressure and its implications in meteorites. American Mineralogist, 101, 205–210, https://doi.org/10.2138/am-2016-5466.

Guillermet, A.F. and Frisk, K. (1991) Thermodynamic properties of Ni nitrides and phase stability in the Ni-N system. International Journal of Thermophysics, 12, 417–431, https://doi.org/10.1007/BF00500762.

Guo, K., Rau, D., von Appen, J., Prots, Y., Schnelle, W., Dronskowski, R., Niewa, R., and Schwarz, U. (2013) High pressure high-temperature behavior and magnetic properties of Fe_4N: Experiment and theory. High Pressure Research, 33, 684–696, https://doi.org/10.1080/08957959.2013.809715.

Halliday, A.N. (2013) The origins of volatiles in the terrestrial planets. Geochimica et Cosmochimica Acta, 105, 146–171, https://doi.org/10.1016/j.gca.2012.11.015.

Hirao, N., Akahama, Y., and Ohishi, Y. (2022) Equations of state of iron and nickel to the pressure at the center of the Earth. Matter and Radiation at Extremes, 7, 038403.

Hou, M., He, Y., Jang, B.G., Sun, S., Zhuang, Y., Deng, L., Tang, R., Chen, J., Ke, F., Meng, Y., and others. (2021) Superionic iron oxide-hydroxide in Earth's deep mantle. Nature Geoscience, 14, 174–178, https://doi.org/10.1038/s41561-021-00696-2.

Ishimatsu, N., Maruyama, H., Kawamura, N., Suzuki, M., Ohishi, Y., Ito, M., Nasu, S., Kawakami, T., and Shimomura, O. (2003) Pressure-induced magnetic transition in Fe_4N probed by Fe K-edge XMCD measurement. Journal of the Physical Society of Japan, 72, 2372–2376, https://doi.org/10.1143/JPSJ.72.2372.

Jack, K.H. (1948) Binary and ternary interstitial alloys-II. The iron-carbon-nitrogen system. Proceedings of the Royal Society A: Mathematical and Physical Sciences, 195, 41–55, https://doi.org/10.1098/rspa.1948.0101.

Javoy, M. (1997) The major volatile elements of the Earth: Their origin, behavior, and fate. Geophysical Research Letters, 24, 177–180, https://doi.org/10.1029/96GL03931.

Johnson, B. and Goldblatt, C. (2015) The nitrogen budget of Earth. Earth-Science Reviews, 148, 150–173, https://doi.org/10.1016/j.earscirev.2015.05.006.

Kaminsky, F. and Wirth, R. (2017) Nitrides and carbonitrides from the lowermost mantle and their importance in the search for Earth's "lost" nitrogen. American Mineralogist, 102, 1667–1676, https://doi.org/10.2138/am-2017-6101.

Kusakabe, M., Hirose, K., Sinmyo, R., Kuwayama, Y., Ohishi, Y., and Helffrich, G. (2019) Melting curve and equation of state of β-Fe_7N_3: Nitrogen in the core? Journal of Geophysical Research: Solid Earth, 124, 3448–3457, https://doi.org/10.1029/2018JB015823.

Lai, X., Zhu, F., Liu, Y., Bi, W., Zhao, J., Alp, E.E., Hu, M.Y., Zhang, D., Tkachev, S., Manghnani, M.H., and others. (2020) Elastic and magnetic properties of Fe_3P up to core pressures: Phosphorus in the Earth's core. Earth and Planetary Science Letters, 531, 115974, https://doi.org/10.1016/j.epsl.2019.115974.

Li, Y., Vočadlo, L., Brodholt, J., and Wood, I.G. (2016) Thermoelasticity of Fe_7C_3 under inner core conditions. Journal of Geophysical Research: Solid Earth, 121, 5828–5837, https://doi.org/10.1002/2016JB013155.

Lin, J.-F., Fei, Y., Sturhahn, W., Zhao, J., Mao, H.-K., and Hemley, R.J. (2004) Magnetic transition and sound velocities of Fe_3S at high pressure: Implications for Earth and planetary cores. Earth and Planetary Science Letters, 226, 33–40, https://doi.org/10.1016/j.epsl.2004.07.018.

Litasov, K.D., Popov, Z.I., Gavryushkin, P.N., Ovchinnikov, S.G., and Fedorov, A.S. (2015) First-principles calculations of the equations of state and relative stability of iron carbides at the Earth's core pressures. Russian Geology and Geophysics, 56, 164–171, https://doi.org/10.1016/j.rgg.2015.01.010.

Litasov, K.D., Shatskiy, A., Ponomarev, D.S., and Gavryushkin, P.N. (2017) Equations of state of iron nitrides ε-Fe_3N_x and γ-Fe_4N_y to 30 GPa and 1200 K and implication for nitrogen in the Earth's core. Journal of Geophysical Research: Solid Earth, 122, 3574–3584, https://doi.org/10.1002/2017JB014059.

Liu, J., Hu, Q., Bi, W., Yang, L., Xiao, Y., Chow, P., Meng, Y., Prakapenka, V.B., Mao, H.-K., and Mao, W.L. (2019) Altered chemistry of oxygen and iron under deep Earth conditions. Nature Communications, 10, 153, https://doi.org/10.1038/s41467-018-08071-3.

Lv, C. and Liu, J. (2022) Ultralow melting of iron nitrides and the Fe-N-C system at high pressure. Journal of Geophysical Research: Solid Earth, 127, e2021JB023718.

——— (2023) The iron spin transition of deep nitrogen-bearing mineral Fe3N1.2 at high pressure. American Mineralogist, 108, 653–658.

Lv, M., Liu, J., Zhu, F., Li, J., Zhang, D., Xiao, Y., and Dorfman, S.M. (2020) Spin transitions and compressibility of ε-Fe_7N_3 and γ'-Fe_4N: Implications for iron alloys in terrestrial planet cores. Journal of Geophysical Research: Solid Earth, 125, e2020JB020660.

Mao, H.-K. and Mao, W.L. (2020) Key problems of the four-dimensional Earth system. Matter and Radiation at Extremes, 5, 038102, https://doi.org/10.1063/1.5139023.

Mao, H.-K., Xu, J., and Bell, P.M. (1986) Calibration of the ruby pressure gauge to 800 kbar under quasi-hydrostatic conditions. Journal of Geophysical Research: Solid Earth, 91, 4673–4676, https://doi.org/10.1029/JB091iB05p04673.

Marty, B., Zimmermann, L., Pujol, M., Burgess, R., and Philippot, P. (2013) Nitrogen isotopic composition and density of the Archean atmosphere. Science, 342, 101–104, https://doi.org/10.1126/science.1240971.

Minobe, S., Nakajima, Y., Hirose, K., and Ohishi, Y. (2015) Stability and compressibility of a new iron nitride β-Fe_7N_3 to core pressures. Geophysical Research Letters, 42, 5206–5211, https://doi.org/10.1002/2015GL064496.

Mookherjee, M. (2011) Elasticity and anisotropy of Fe_3C at high pressures. American Mineralogist, 96, 1530–1536, https://doi.org/10.2138/am.2011.3917.

Moore, C.B., Gibson, E.K. Jr., and Keil, K. (1969) Nitrogen abundances in enstatite chondrites. Earth and Planetary Science Letters, 6, 457–460, https://doi.org/10.1016/0012-821X(69)90116-2.

Ohta, K., Kuwayama, Y., Hirose, K., Shimizu, K., and Ohishi, Y. (2016) Experimental determination of the electrical resistivity of iron at Earth's core conditions. Nature, 534, 95–98, https://doi.org/10.1038/nature17957.

Panda, R.N. and Gajbhiye, N.S. (1997) Magnetic properties of single domain ε-Fe_3N synthesized by borohydride reduction route. Journal of Applied Physics, 81, 335–339, https://doi.org/10.1063/1.364115.

Pepin, R.O. (2006) Atmospheres on the terrestrial planets: Clues to origin and evolution. Earth and Planetary Science Letters, 252, 1–14, https://doi.org/10.1016/j.epsl.2006.09.014.

Popov, Z.I., Litasov, K.D., Gavryushkin, P.N., Ovchinnikov, S.G., and Fedorov, A.S. (2015) Theoretical study of γ′-Fe_4N and ε-Fe_xN iron nitrides at pressures up to 500 GPa. JETP Letters, 101, 371–375, https://doi.org/10.1134/S0021364015060090.

Prescher, C. and Prakapenka, V.B. (2015) DIOPTAS: A program for reduction of two-dimensional X-ray diffraction data and data exploration. High Pressure Research, 35, 223–230, https://doi.org/10.1080/08957959.2015.1059835.

Prescher, C., Dubrovinsky, L., McCammon, C., Glazyrin, K., Nakajima, Y., Kantor, A., Merlini, M., and Hanfland, M. (2012) Structurally hidden magnetic transitions in Fe_3C at high pressures. Physical Review B: Condensed Matter and Materials Physics, 85, 140402, https://doi.org/10.1103/PhysRevB.85.140402.

Prescher, C., Dubrovinsky, L., Bykova, E., Kupenko, I., Glazyrin, K., Kantor, A., McCammon, C., Mookherjee, M., Nakajima, Y., Miyajima, N., and others. (2015) High Poisson's ratio of Earth's inner core explained by carbon alloying. Nature Geoscience, 8, 220–223, https://doi.org/10.1038/ngeo2370.

Rohrbach, A., Ballhaus, C., Golla-Schindler, U., Ulmer, P., Kamenetsky, V.S., and Kuzmin, D.V. (2007) Metal saturation in the upper mantle. Nature, 449, 456–458, https://doi.org/10.1038/nature06183.

Rohrbach, A., Ghosh, S., Schmidt, M.W., Wijbrans, C.H., and Klemme, S. (2014) The stability of Fe-Ni carbides in the Earth's mantle: Evidence for a low Fe-Ni-C melt fraction in the deep mantle. Earth and Planetary Science Letters, 388, 211–221, https://doi.org/10.1016/j.epsl.2013.12.007.

Sagatov, N., Gavryushkin, P.N., Inerbaev, T.M., and Litasov, K.D. (2019) New high-pressure phases of Fe_7N_3 and Fe_7C_3 stable at Earth's core conditions: Evidences for carbon-nitrogen isomorphism in Fe-compounds. RSC Advances, 9, 3577–3581, https://doi.org/10.1039/C8RA09942A.

Schwarz, U., Wosylus, A., Wessel, M., Dronskowski, R., Hanfland, M., Rau, D., and Niewa, R. (2009) High-pressure-high-temperature behavior of ζ-Fe_2N and phase transition to ε-$Fe_3N_{1.5}$. European Journal of Inorganic Chemistry, 2009, 1634–1639, https://doi.org/10.1002/ejic.200801222.

Seagle, C.T., Cottrell, E., Fei, Y., Hummer, D.R., and Prakapenka, V.B. (2013) Electrical and thermal transport properties of iron and iron-silicon alloy at high pressure. Geophysical Research Letters, 40, 5377–5381, https://doi.org/10.1002/2013GL057930.

Shi, L., Lu, W., Kagoshima, T., Sano, Y., Gao, Z., Du, Z., Liu, Y., Fei, Y., and Li, Y. (2022) Nitrogen isotope evidence for Earth's heterogeneous accretion of volatiles. Nature Communications, 13, 4769, https://doi.org/10.1038/s41467-022-32516-5.

Sífkovits, M., Smolinski, H., Hellwig, S., and Weber, W. (1999) Interplay of chemical bonding and magnetism in Fe_4N, Fe_3N and ζ-Fe_2N. Journal of Magnetism and Magnetic Materials, 204, 191–198, https://doi.org/10.1016/S0304-8853(99)00296-6.

Sokol, A.G., Kruk, A.N., Seryotkin, Y.V., Korablin, A.A., and Palyanov, Y.N. (2017a) Phase relations in the Fe-Fe_3C-Fe_3N system at 7.8 GPa and 1350 °C: Implications for carbon and nitrogen hosts in Fe^0-saturated upper mantle. Physics of the Earth and Planetary Interiors, 265, 43–53, https://doi.org/10.1016/j.pepi.2017.02.007.

Sokol, A.G., Palyanov, Y.N., Tomilenko, A.A., Bul'bak, T.A., and Palyanova, G.A. (2017b) Carbon and nitrogen speciation in nitrogen-rich C-O-H-N fluids at 5.5–7.8 GPa. Earth and Planetary Science Letters, 460, 234–243, https://doi.org/10.1016/j.epsl.2016.11.050.

Stacey, F.D. and Loper, D.E. (2007) A revised estimate of the conductivity of iron alloy at high pressure and implications for the core energy balance. Physics of the Earth and Planetary Interiors, 161, 13–18, https://doi.org/10.1016/j.pepi.2006.12.001.

Strong, H.M. and Chrenko, R.M. (1971) Diamond growth rates and physical properties of laboratory-made diamond. Journal of Physical Chemistry, 75, 1838–1843, https://doi.org/10.1021/j100681a014.

Sturhahn, W. (2004) Nuclear resonant spectroscopy. Journal of Physics Condensed Matter, 16, S497–S530, https://doi.org/10.1088/0953-8984/16/5/009.

Suehiro, S., Ohta, K., Hirose, K., Morard, G., and Ohishi, Y. (2017) The influence of sulfur on the electrical resistivity of hcp iron: Implications for the core conductivity of Mars and Earth. Geophysical Research Letters, 44, 8254–8259, https://doi.org/10.1002/2017GL074021.

Sugiura, N., Kiyota, K., and Hashizume, K. (1998) Nitrogen components in primitive ordinary chondrites. Meteoritics & Planetary Science, 33, 463–482, https://doi.org/10.1111/j.1945-5100.1998.tb01651.x.

van der Pauw, L.J. (1958) A method of measuring specific resistivity and Hall effect of discs of arbitrary shape. Philips Research Reports, 13, 1–9.

Watenphul, A., Wunder, B., Wirth, R., and Heinrich, W. (2010) Ammonium-bearing clinopyroxene: A potential nitrogen reservoir in the Earth's mantle. Chemical Geology, 270, 240–248, https://doi.org/10.1016/j.chemgeo.2009.12.003.

Widenmeyer, M., Hansen, T.C., Meissner, E., and Niewa, R. (2014) Formation and decomposition of iron nitrides observed by in situ powder neutron diffraction and thermal analysis. Zeitschrift für Anorganische und Allgemeine Chemie, 640, 1265–1274, https://doi.org/10.1002/zaac.201300676.

Ye, Y., Shim, S.-H., Prakapenka, V., and Meng, Y. (2018) Equation of state of solid Ne inter-calibrated with the MgO, Au, Pt, NaCl-B2, and ruby pressure scales up to 130 GPa. High Pressure Research, 38, 377–395, https://doi.org/10.1080/08957959.2018.1493477.

Yin, W., Lei, L., Jiang, X., Liu, P., Liu, F., Li, Y., Peng, F., and He, D. (2014) High pressure synthesis and properties studies on spherical bulk ε-Fe_3N. High Pressure Research, 34, 317–326, https://doi.org/10.1080/08957959.2014.944910.

Zerkle, A.L. and Mikhail, S. (2017) The geobiological nitrogen cycle: From microbes to the mantle. Geobiology, 15, 343–352, https://doi.org/10.1111/gbi.12228.

Zhang, C., Lin, J.-F., Liu, Y., Feng, S., Jin, C., Hou, M., and Yoshino, T. (2018) Electrical resistivity of Fe-C alloy at high pressure: Effects of carbon as a light element on the thermal conductivity of the Earth's core. Journal of Geophysical Research: Solid Earth, 123, 3564–3577, https://doi.org/10.1029/2017JB015260.

Zhuang, Y., Su, X., Salke, N.P., Cui, Z., Hu, Q., Zhang, D., and Liu, J. (2021) The effect of nitrogen on the compressibility and conductivity of iron at high pressure. Geoscience Frontiers, 12, 983–989, https://doi.org/10.1016/j.gsf.2020.04.012.

Zhuang, Y., Gan, B., Cui, Z., Tang, R., Tao, R., Hou, M., Jiang, G., Popescu, C., Garbarino, G., Zhang, Y., and others. (2022) Mid-mantle water transportation implied by the electrical and seismic properties of ε-FeOOH. Science Bulletin, 67, 748–754, https://doi.org/10.1016/j.scib.2021.12.002.

Manuscript received November 15, 2023
Manuscript accepted July 20, 2024
Accepted manuscript online August 6, 2024
Manuscript Handled by Bin Chen

Endnotes:

[1]Deposit item AM-25-49251. Online Materials are free to all readers. Go online, via the table of contents or article view, and find the tab or link for supplemental materials.